Supporting Information

Mixed-Chloride Additives Control the Quality and Control by Mixed-Chloride Additives of the Quality and Homogeneity of Bulk Halide Perovskite upon Film Formation Process.

*Daming Zheng and Thierry Pauporté**

Chimie ParisTech, PSL Research University, CNRS, Institut de Recherche de Chimie Paris (IRCP), UMR8247, 11 rue P. et M. Curie, F-75005 Paris, France.

*Corresponding author, email: thierry.pauporte@chimieparistech.psl.eu

Website: www.pauportegroup.com

Table S1 Review of the MA-free perovskite and corresponding device configuration of PSCs with PCE > 20% published in the literature.

Perovskite (Concentration of PbI_2)	Device configuration	Stabilized PCE	Ref.
$Cs_{0.1}FA_{0.9}PbI_3$ (1.0 M)	FTO/TiO_2/PVK/spiro-OMeTAD/Au	21.03%	Our work
$Cs_{0.1}FA_{0.9}PbI_3$ (1.3 M)	ITO/SnO_2/PVK/spiro-OMeTAD/PTAA/Au	20.12%	[1]
$Cs_{0.15}FA_{0.85}Pb(I_{0.9}Br_{0.1})_3$ (1.2 M)	FTO/TiO_2/PVK/spiro-OMeTAD/Au	20.5%	[2]
$Cs_{0.05}FA_{0.95}PbI_3$ (1.4 M)	ITO/E-SnO_2/PVK/spiro-OMeTAD/Au	21.67%	[3]
$Cs_{0.1}FA_{0.9}PbI_3$ (1.4 M)	FTO/TiO_2/PVK/YZ22/Au	22.3%	[4]
$Rb_{0.05}Cs_{0.1}FA_{0.85}PbI_3$ (1.1 M)	ITO/ PCBM:PMMA/PVK/spiro-OMeTAD/Au	20.35%	[5]
$Rb_{0.05}Cs_{0.1}FA_{0.85}PbI_3$ (1.1 M)	ITO/SnO_2/PVK/spiro-OMeTAD/Au	20.9%	[6]

Reference

[1] N. Li, Y. Luo, Z. Chen, X. Niu, X. Zhang, J. Lu, R. Kumar, J. Jiang, H. Liu, X. Guo, B. Lai, Geert Brocks, Q. Chen, S. Tao, David P. Fenning and H. Zhou, *Joule*, 2020, **4**, 1-16.

[2] J. Yang, Y. Chen, W. Tang, S. Wang, Q. Ma, Y. Wu, N. Yuan, J. Ding and W. Zhang, *J. Energy Chem.*, 2020, **48**, 217–225.

[3] D. Yang, R. Yang, K. Wang, C. Wu, X. Zhu, J. Feng, X. Ren, G. Fang, S. Priya and S. Liu, *Nat. Commun.*, 2018, **9**, 3239.

[4] X. Zhao, C. Yao, K. Gu, T. Liu, Y. Xia and Y. Loo, *Energy Eenviron. Sci.*, 2020, **13**, 4334-4343.

[5] S. Turren-Cruz, A. Hagfeldt and M. Saliba, *Science*, 2018, **362**, 449-453.

[6] S. Li, Z. Liu, Z. Qiao, X. Wang, L. Cheng, Y. Zhai, Q. Xu, Z. Li, K. Meng and G. Chen, *Adv. Funct. Mater.*, 2020, 2005846

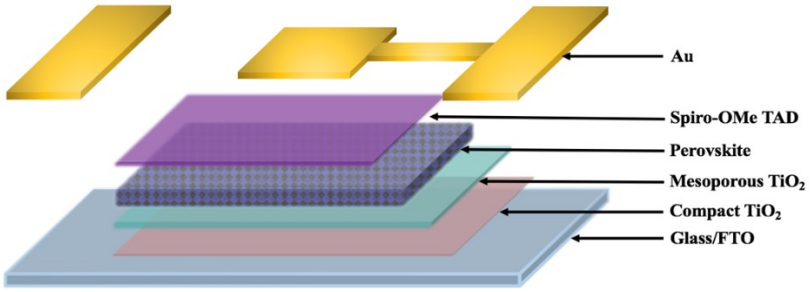

Figure S1. Schematic exploded view of the perovskite solar cell structure.

A. NH_4Cl additive for $Cs_{0.1}FA_{0.9}PbI_3$.

We have supposed that ammonium chloride (NH_4Cl, AC samples) additive should present the advantage to mediate the layer growth, while being fully eliminated at the end of the synthesis, upon the annealing step performed at 155°C for 20 min. We prepared $Cs_{0.1}FA_{0.9}PbI_3$ layers with NH_4Cl additive in the precursor solution varying between 10 mol% to 50 mol% of the molar content of PbI_2 (noted AC-10 to AC-50 samples). They have been compared to pristine layers (noted REF). SEM top-views images of the REF film presented pinholes and many bright grains dispersed onto the surface corresponding to PbI_2 (**Figure S2a**). The perovskite grains were rather small with a mean size measured at ~400 nm. Adding AC at 10 mol% was beneficial since the pinholes were eliminated and the quantity of PbI_2 was reduced (**Figure S2b**). Increasing NH_4Cl up to 30 mol% led to a continuous enlargement of the perovskite grain size (**Figure S2c, S2d** and **S2e**). Then, the grain size decreased. Moreover, at 50 mol%, pinholes were present again (**Figure S2f**). **Figure S2g** discloses the statistical grain size analysis done with the Image J software. The highest mean grain size was recorded for AC-30 at ~750 nm mean value. XRD patterns in **Figure S3**, show that all the films were texturised with the (001) plane parallel to the substrate. The perovskite diffraction peak intensity increased up to AC-30 and then diminished. PbI_2 parasitic phase was present whatever the concentration of AC employed. The relative intensity of the

PbI_2 diffraction peaks compared to the perovskite ones was only slightly reduced by the AC additive. The samples absorbance spectra in **Figure S4a** show that the AC-30 sample exhibited the best absorbance and that the absorption edge was unchanged with the additive amount. The minimum of PL intensity was measured for the AC-30 layer (**Figure S4b**,). It corresponds to sample with the best quenching due to an excellent charge transfer towards the TiO_2 substrate.

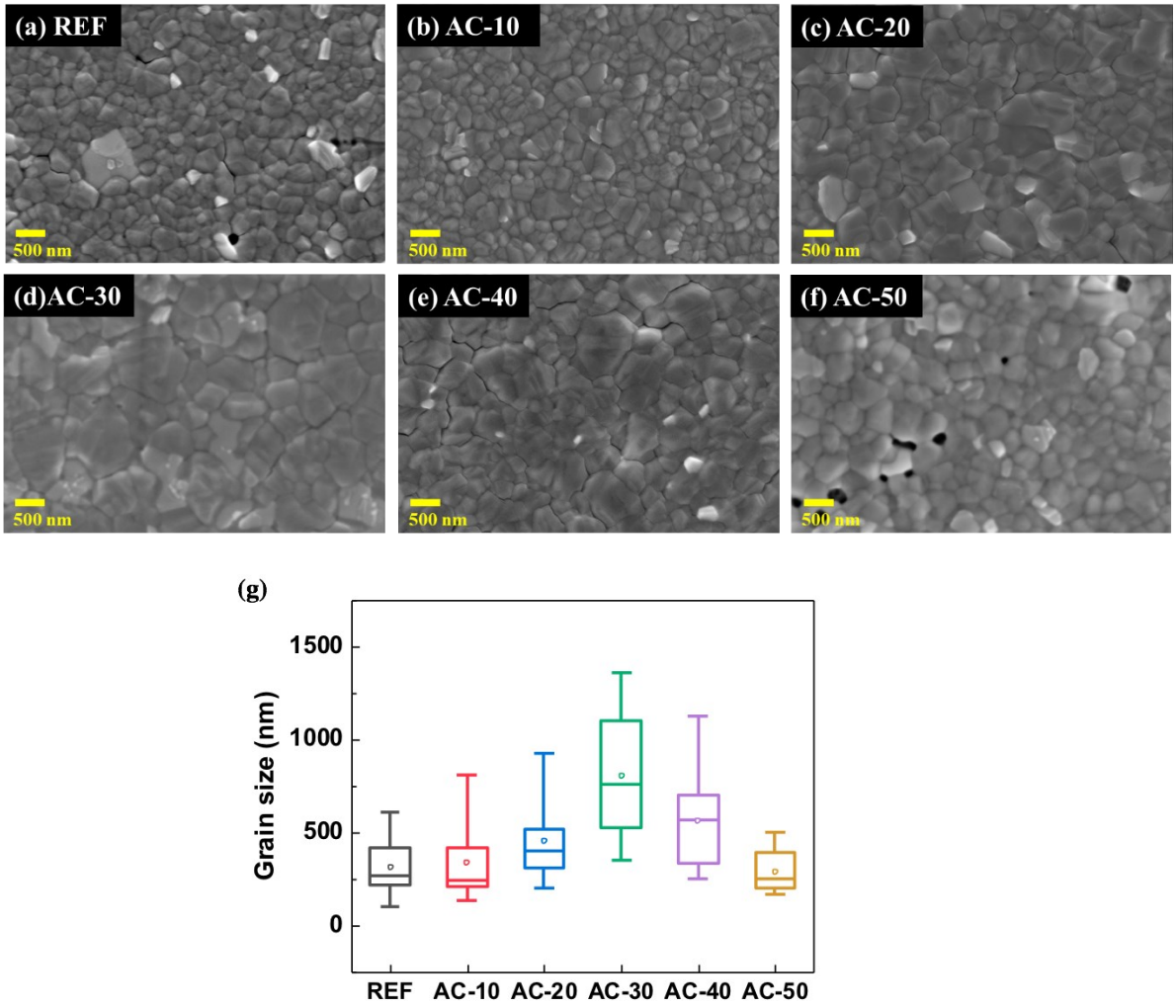

Figure S2. SEM top view images of $Cs_{0.1}FA_{0.9}PbI_3$ layers prepared with increasing amount of ammonium chloride (AC) additive: (a) REF, (b) AC-10, (c) AC-20, (d) AC-30, (e) AC-40 and (f) AC-50. The scale bar is 500 nm. (g) Statistical analysis of the grain size.

From all these characterizations, we deduced that the AC-30 sample exhibited the best morphological, structural and optical properties for PSC application. This was confirmed by PSC performances measurements with AC-30 cells reaching the best PCE (**Figure S5)**.

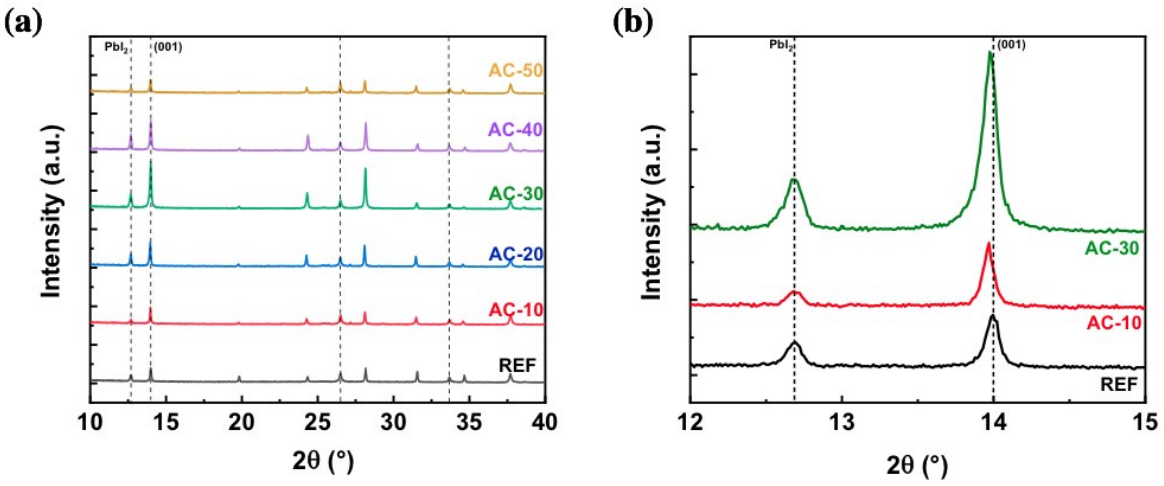

Figure S3. XRD patterns of pristine $Cs_{0.1}FA_{0.9}PbI_3$ layer (REF) and $Cs_{0.1}FA_{0.9}PbI_3$ layers prepared with various AC additive amount. (b) is an enlarged view of (a).

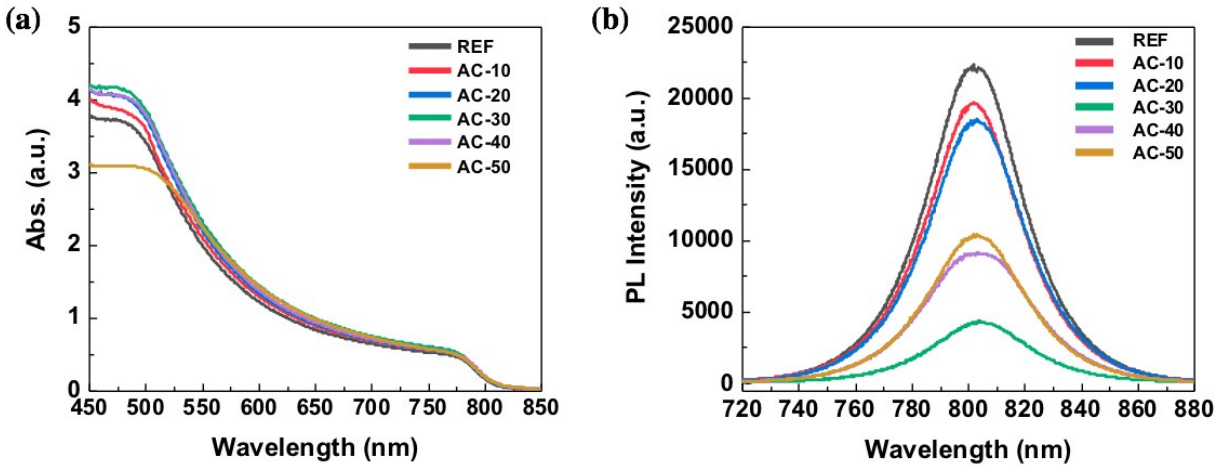

Figure S4. Effect of ammonium chloride additive on the (a) absorbance and (b) steady-state photoluminescence of the layers deposited on the FTO/c-TiO_2/mp-TiO_2 layers' substrate.

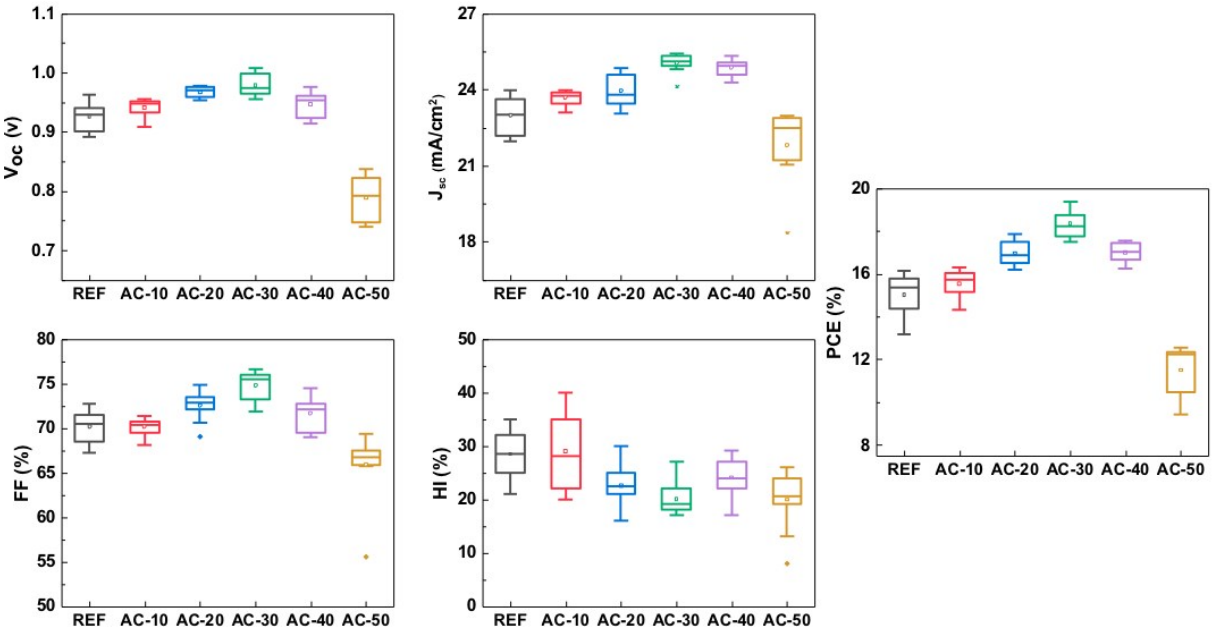

Figure S5. Statistical analysis of the effect of AC additive on the *J-V* curve parameters: open circuit voltage (V_{oc}), short circuit current density (J_{sc}), fill factor (FF), power conversion hysteresis (PCE) and hysteresis index (HI) defined as : $HI(\%)=(PCE_{reverse}-PCE_{forward})*100/PCE_{reverse}$.

B- KCl additive for $Cs_{0.1}FA_{0.9}PbI_3$.

We have first investigated the beneficial effects of potassium chloride (KCl) on the properties and performances of $Cs_{0.1}FA_{0.9}PbI_3$. KCl additive cannot be used in a large amount because K^+ is not eliminated upon annealing at 150°C and it remains in the layer. Moreover, the solubility of potassium chloride in the precursor solution is quite limited. Consequently, we investigated precursor solutions with KCl at 0 mol%, 5 mol%, 9 mol% and 13 mol% of the molar PbI_2 content and are noted w/o, KC-5, KC-9 and KC-13, respectively. The scanning electron microscopy (SEM) images of the resulting layers are shown in **Figure S6.** KCl additive prevents the formation of pinholes and of bright grains that are assigned to PbI_2. XRD measurements (**Figure S6e)**, show that this additive does not improve the crystallinity, but the obtained compounds are α-$Cs_{0.1}FA_{0.9}PbI_3$ pure phase. The absence of PbI_2 is assigned to a better solubilization of PbI_2 in DMF/DMSO solvent mixture in the presence of this additive. **Figure S7a** reveals the best measured absorbance for 9 mol% and the PL spectra (**Figure S7b)** indicate the lowest intensity for this sample for which the best charge transfer toward the TiO_2 front electron selective contact occurs. The statistical analysis of PSC prepared with various amounts of KCl is disclosed in **Figure S8**. The maximum PCE was achieved for 9 mol% KCl at 19.16% which is a marked improvement compared to 16.13% for the control. A very interesting observation is that, compared to the pristine cell (REF), employing KCl additive suppressed the *J-V* curves hysteresis.

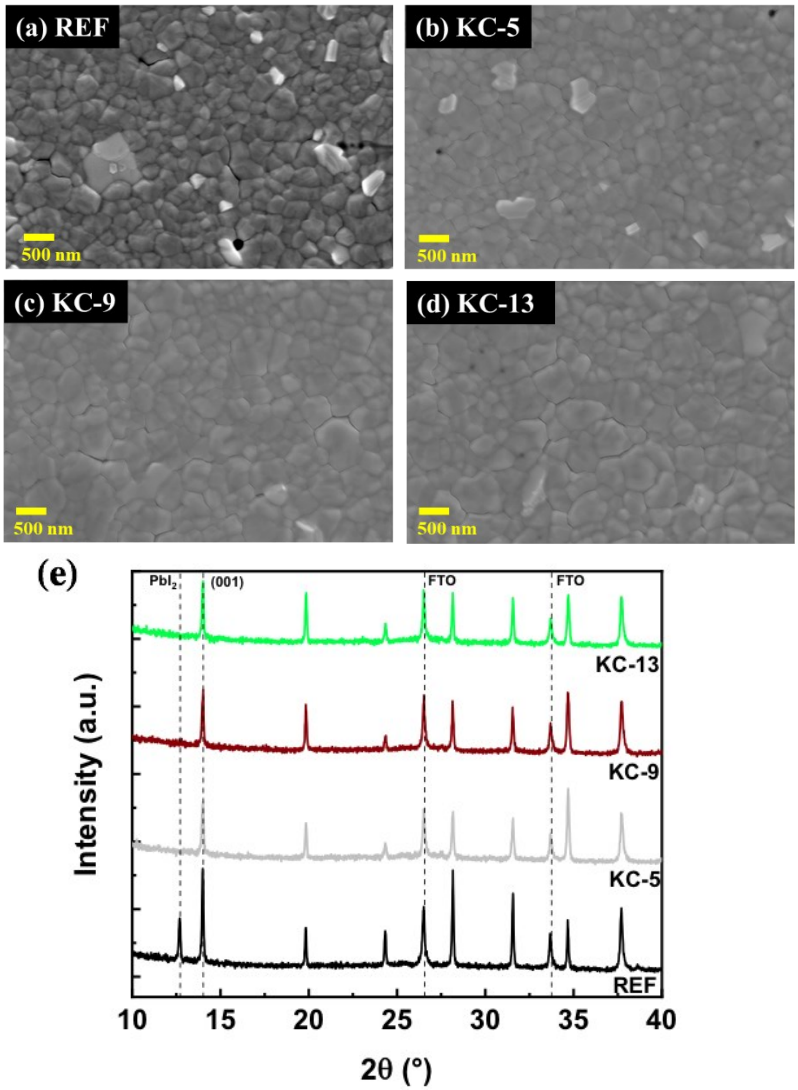

Figure S6. (a-d) SEM top view images of $Cs_{0.1}FA_{0.9}PbI_3$ layers prepared with increasing amount of potassium chloride additive: (a) REF, (b) KC-5, (c) KC-9 and (d) KC-13. (e) XRD patterns of pristine $Cs_{0.1}FA_{0.9}PbI_3$ layer and $Cs_{0.1}FA_{0.9}PbI_3$ layers prepared with various AC additive amount.

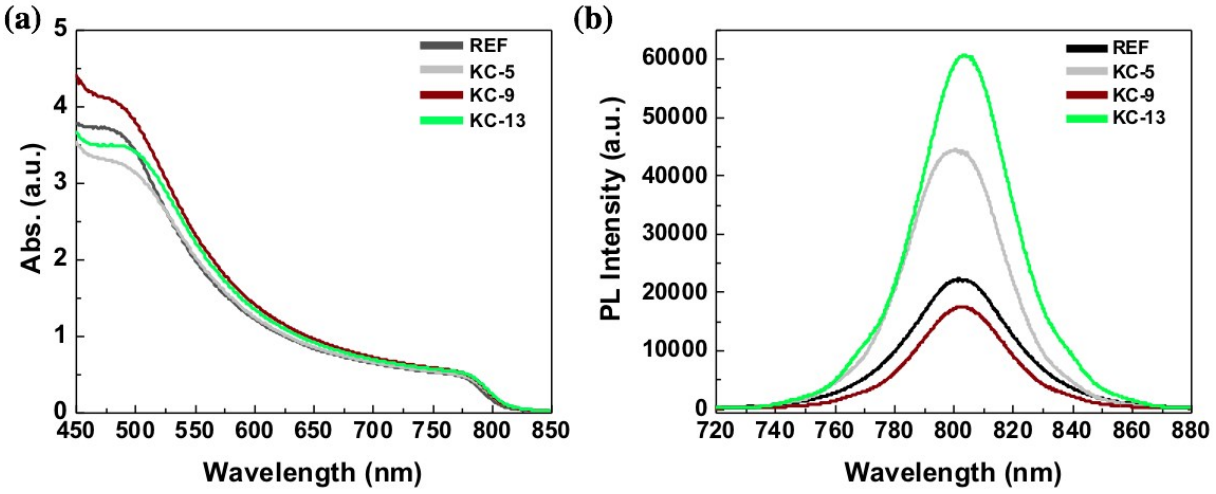

Figure S7. Effect of potassium chloride additive on the (a) absorbance and (b) steady-state photoluminescence spectra of the layers deposited onto the FTO/c-TiO_2/mp-TiO_2 layers' substrate.

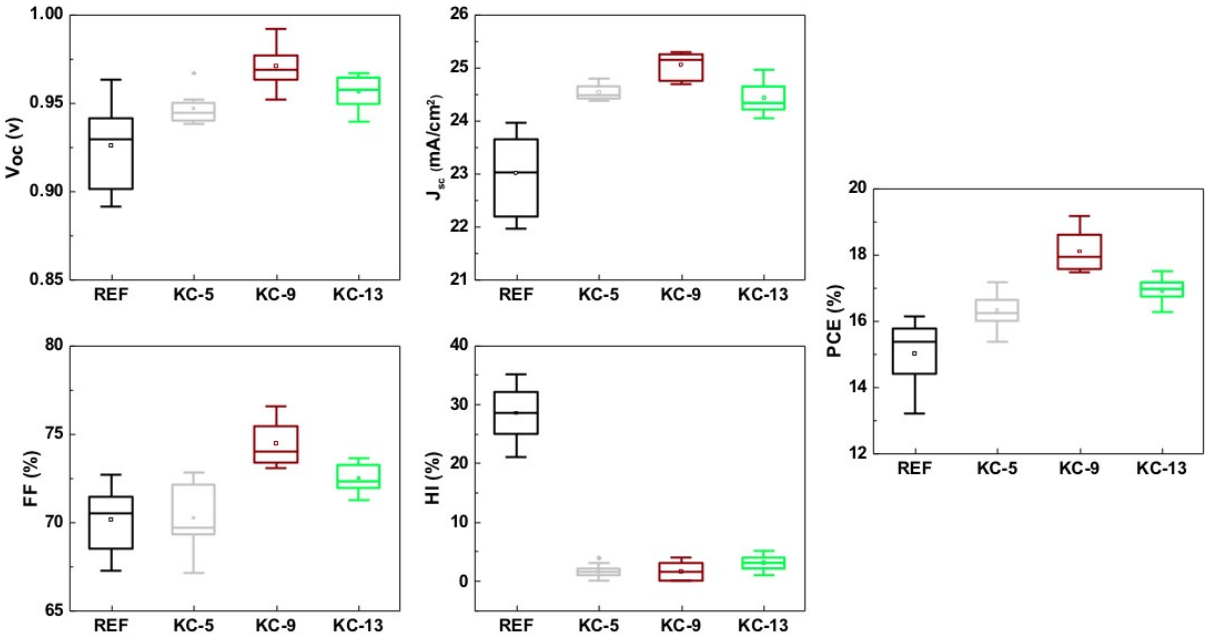

Figure S8. Statistical analysis of the effect of KC additive on the *J-V* curve parameters.

C. NH_4Cl and KCl mixed additive for $Cs_{0.1}FA_{0.9}PbI_3$.

Having shown that both additives are of high interest, we then investigated their mixture to combine their beneficial effect. Four different mixtures were notably investigated which kept the total amount of chloride ion between 25 mol% and 39 mol% of PbI_2 molar amount in the PPS. The studied films are noted AC-20/KC-5, AC-30/KC-5, AC-20/KC-9 and AC-30/KC-9. **Figure S9** displays the statistical analysis of the PSCs prepared with different amounts of additive mixtures. An optimum of the three *J-V* curve parameters, namely the open circuit voltage (V_{oc}), the short circuit current (J_{sc}) and the fill factor (*FF*) was found for AC-30/KC-5 (see also **Table S2**, Supporting Information).

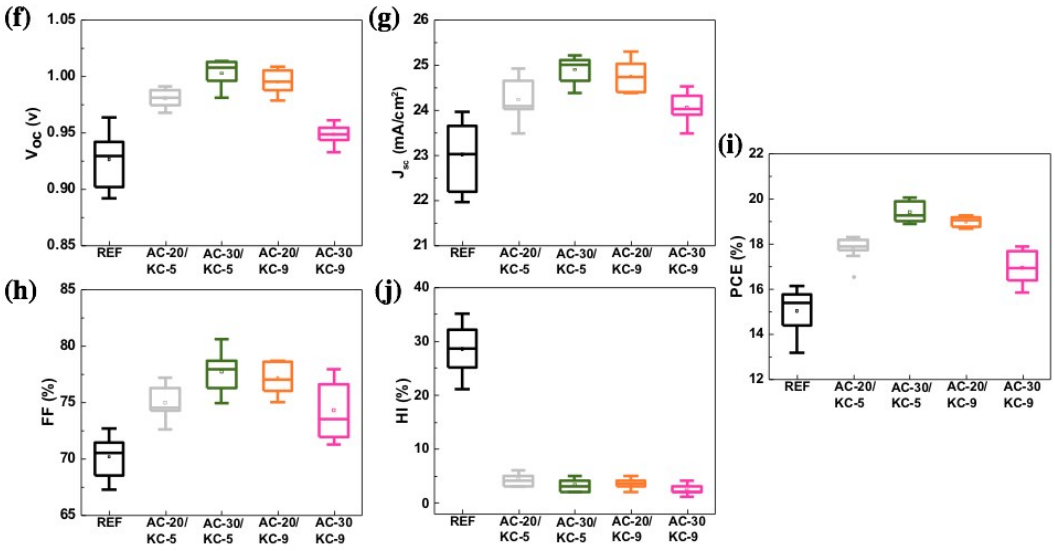

Figure S9. Statistical analysis of the effect of combining various NH_4Cl and KCl additives mol% on the *J-V* curve parameters of PSCs. (f) V_{oc}, (g) J_{sc}, (h) *FF*, (i) PCE and (j) hysteresis index defined as *HI*(%) = $[PCE_{rev}-PCE_{for}]*100/PCE_{rev}$

Table S2. *J-V* curves parameters, PCE and HI of $Cs_{0.1}FA_{0.9}PbI_3$ PSCs prepared with different amount of AC and KC additives

No.	Entry	V_{oc} [V]	J_{sc} [mA cm^{-2}]	FF [%]	PCE [%]	HI [%]
REF	Reverse	0.941	23.82	71.92	16.13	28
	Forward	0.837	23.88	58.24	11.65	
AC-20/ KC-5	Reverse	0.984	24.65	75.34	18.27	4
	Forward	0.976	24.34	75.14	17.58	
AC-30/KC-5	Reverse	1.012	25.21	78.61	20.05	3
	Forward	1.013	24.94	76.73	19.39	
AC-20/ KC-9	Reverse	1.005	24.39	78.53	19.24	2
	Forward	1.004	24.17	77.84	18.89	
AC-30/ KC-9	Reverse	0.947	24.31	77.69	17.88	2
	Forward	0.951	24.19	76.64	17.63	

Table S3. Champion and average of a minimum of 15 cells (in bracket) $Cs_{0.1}FA_{0.9}PbI_3$ solar cells *J-V* curve parameters, PCE and hysteresis index.

Name	Additive	Capping layer	Scan direction	V_{oc} [V]	J_{sc} [mA. cm^{-2}]	*FF*	PCE [%]	*HI(%)*[a)]
REF	No	No	Reverse	0.943 (0.932)	23.91 (23.07)	72.13 (71.90)	16.26 (15.45)	26 (28.3)
			Forward	0.846 (0.842)	23.83 (23.02)	59.36 (57.11)	11.96 (11.07)	
AC	NH_4Cl 30 mol%	No	Reverse	1.004 (0.971)	25.32 (25.12)	76.08 (76.03)	19.34 (18.54)	18 (19.4)
			Forward	0.957 (0.926)	25.13 (24.93)	66.07 (64.79)	15.89 (14.95)	
KC	KCl 9 mol%	No	Reverse	0.994 (0.973)	25.19 (25.08)	76.38 (73.86)	19.12 (17.93)	1 (2.6)
			Forward	0.995 (0.975)	25.16 (24.67)	76.03 (72.59)	19.03 (17.46)	
AKC	NH_4Cl 30 mol% + KCl 5mol%	No	Reverse	1.014 (1.011)	25.23 (25.01)	78.69 (77.63)	20.13 (19.62)	4 (3.6)
			Forward	1.012 (1.007)	24.96 (24.87)	76.84 (75.54)	19.41 (18.91)	
AKC-PAI	NH_4Cl 30 mol% + KCl 5mol%	Yes (4 mg/mL PAI)	Reverse	1.051 (1.048)	25.31 (25.18)	79.23 (78.87)	21.08 (20.61)	3 (3.3)
			Forward	1.049 (1.045)	25.02 (24.95)	77.91 (76.39)	20.45 (19.92)	

[a)] Hysteresis Index, noted HI, defined as $(PCE_{Rev}-PCE_{For})*100/PCE_{Rev}$

D. $Cs_{0.1}FA_{0.9}PbI_3$ film surface treatment.

The next step was to implement additional engineering to improve the PVK/HTL interface. The formation of a capping layer on PVK by its surface treatment is classically employed to boost the PSC performances. The strategy of using a variety of ammonium compounds which react with the 3D perovskite and form a 2D perovskite layer appears as especially promising. We have focused our attention on propylamine hydroiodide (PAI). The effect of spin-coating a solution of PAI at various concentration in isopropyl alcohol (IPA) solvent on the *J-V* curves is disclosed in **Table S3** (Supporting Information). An improvement of the performances was found for all the investigated concentrations. The best result was obtained for 4 mg.mL^{-1} with a PCE that reached 21.08% (**Figure S10**, **Table 1**). The optimized treated films are noted AKC-PAI, hereafter. The beneficial effect of KCl additive was

preserved since the hysteresis remained negligible with HI at 3% (**Table S4**). The statistical analysis (**Figure S10**, Supporting Information) figures out that this treatment mainly improves the cell V_{oc} and the *FF*, while the J_{sc} is unchanged at a high value. It reduces the charge recombination at the PVK/HTL interface. The external quantum efficiency (EQE) spectra and integrated current density of the REF, AKC and AKC-PAI cells are plotted as a function of the wavelength in **Figure S10f.** Both J_{sc}, calculated and measured on the *J-V* curves, are in good agreement. The significant improvement was confirmed by measuring the steady-state PCE (**Figure 1b**) which achieved 21.03% for AKC-PAI, a value very close to the one measured on the *J-V* curve and gained 1% absolute compared to the untreated AKC cells.

Table S4. Effect of PAI concentration in IPA on the *J-V* curves parameters of AKC-PAI cells.

Name	Scan direction	V_{oc} [V]	J_{sc} [mA.cm^{-2}]	FF [%]	PCE [%]	HI [%]
REF	Reverse	1.014	25.23	78.69	20.13	4
	Forward	1.012	24.96	76.84	19.41	
2 mg/mL	Reverse	1.034	25.12	78.88	20.48	4
	Forward	1.035	24.98	76.07	19.67	
3 mg/mL	Reverse	1.045	25.24	78.54	20.72	1
	Forward	1.046	25.17	77.03	20.28	
4 mg/mL	Reverse	1.051	25.31	79.23	21.08	3
	Forward	1.049	25.02	77.91	20.45	
5 mg/mL	Reverse	1.043	24.89	77.61	20.15	2
	Forward	1.042	24.74	76.73	19.78	

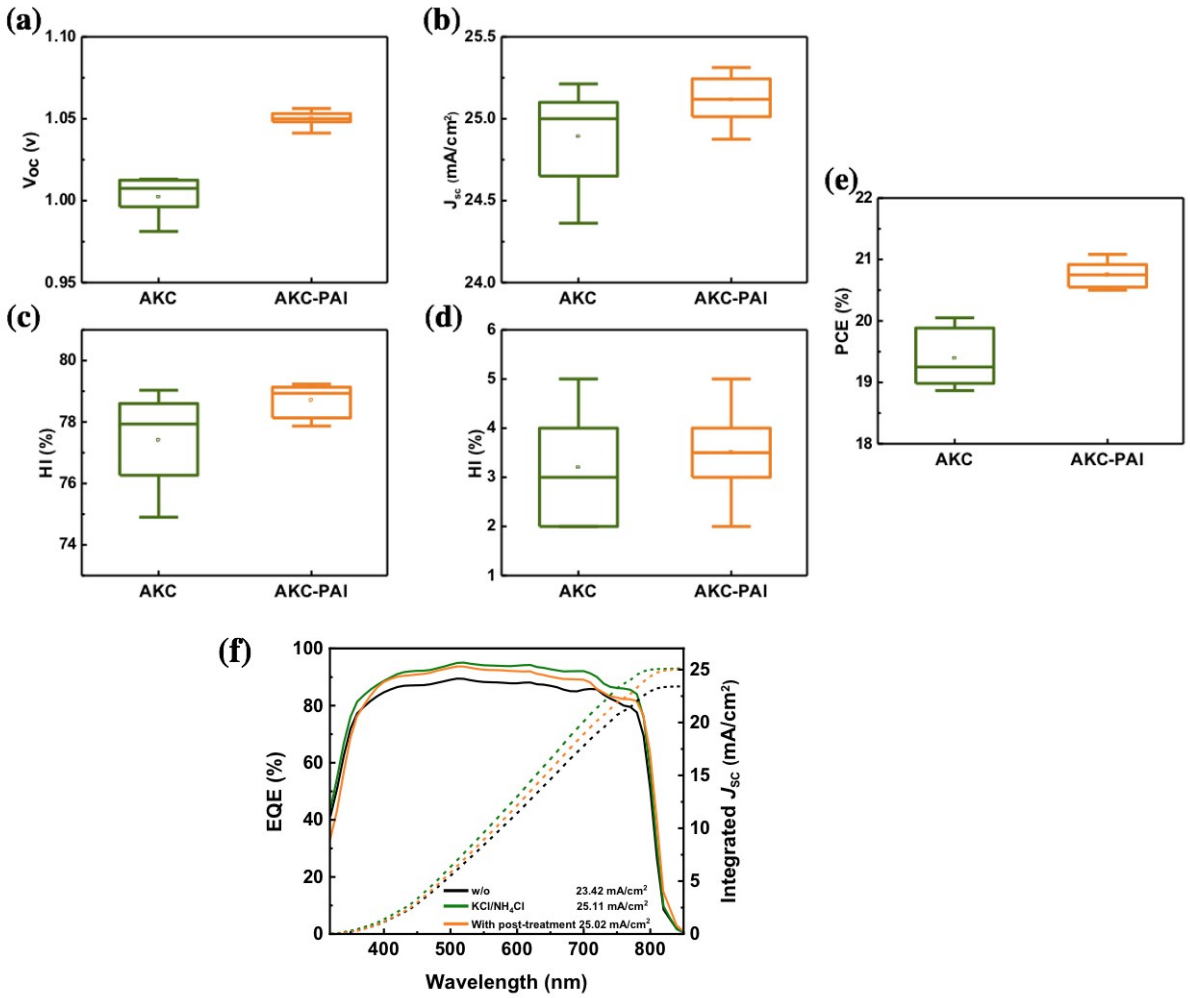

Figure S10. (a-e) Statistical analysis of the *J-V* curve parameters with (AKC-PAI) and without (AKC) PAI post-treatment. (4mg.mL-1 PAI concentration in IPA). (f) EQE spectra and integrated J_{sc} curves.

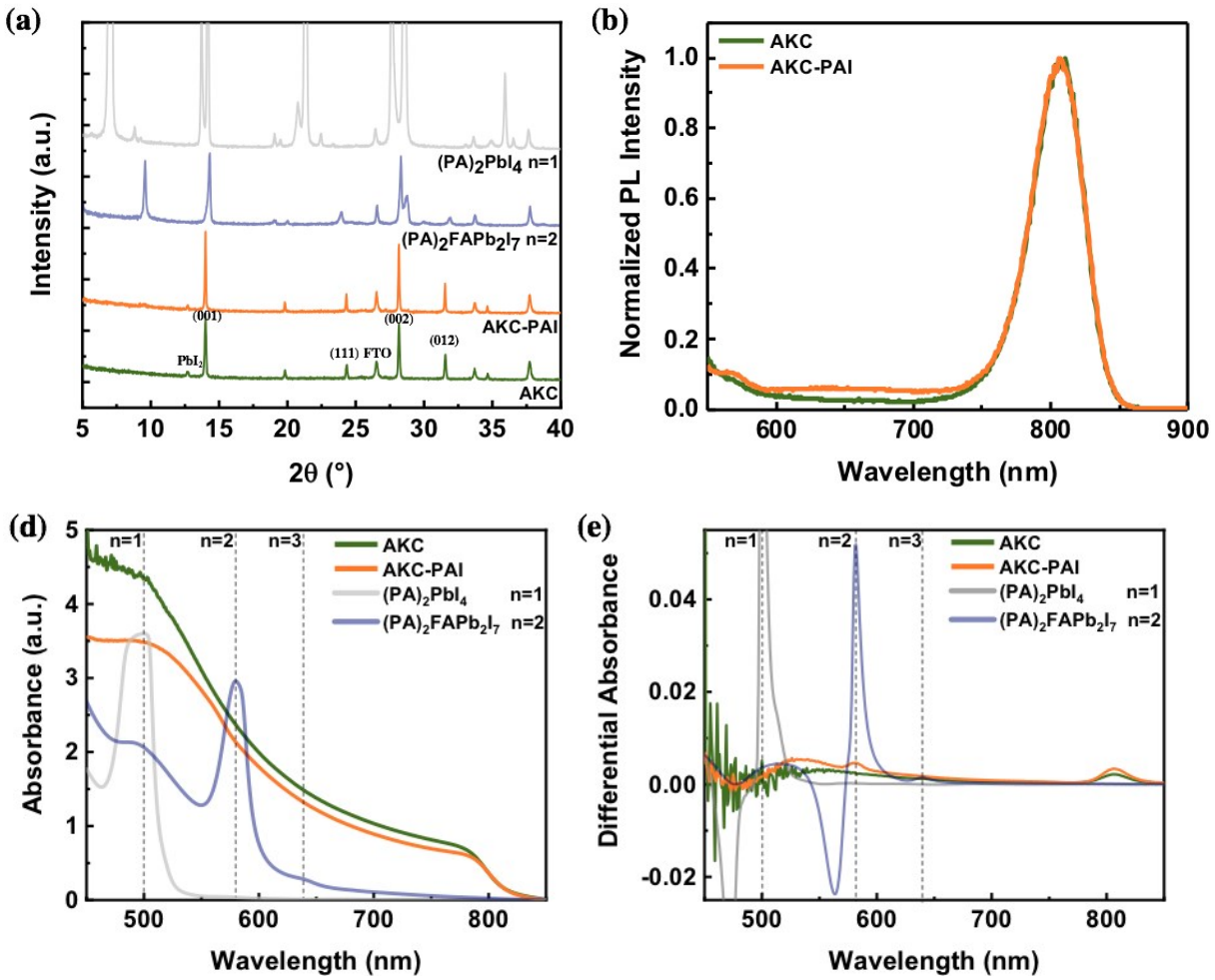

Figure S11. Effect of AKC film post-treatment on (a) XRD pattern and (b) photoluminescence spectrum. The same sample was measured before and after the treatment. (a) is completed by the XRD patterns of $(PA)_2PbI_4$ (n=1) and $(PA)_2FAPbI_7$ (n=2) reference 2D layers. (c) absorbance spectra and (d) absorbance differential spectra of AKC layers before and after the PAI treatment. Comparison with $(PA)_2PbI_4$ (n=1) and $(PA)_2FAPbI_7$ (n=2) reference 2D layers.

The PVK layer surface was altered after the PAI post-growth treatment with the formation of the capping layer (**Figure 1c,d**). This change was clearly visible at the grain boundaries with the presence of an extra-phase. The XRD patterns of a AKC sample before and after the PAI treatment are compared in **Figure 1e** and **S11a**. PAI did not react with PbI_2 since the PbI_2 peak at 12.7° was unchanged. On the other hand, the PVK peaks intensity increased. The treatment resulted in a recrystallization and quality improvement of the PVK. It also caused the appearance of a small extra-XRD peak at 9.53° (**Figure 1e**). Based on the reference XRD patterns displayed in **Figure S11a** (Supporting Information), it is assigned to the (040) reflection of the 2D $(PA)_2FAPb_2I_7$ (n=2) compound. We measured the absorbance spectra of the films before and after the treatment. In **Figure S11c**, the absorbance of the latter is slightly reduced in agreement with the slight reduction of the EQE (**Figure S10f**). To reveal the absorbance contribution of the capping layer, we plotted the curve derivative (**Figure S11e**). The differential

absorbance presented a peak at 580 nm. This peak was indexed based on the absorbance curve of reference 2D layers prepared with n=1 and n=2 stoichiometries. Their absorbance curve presented a main peak at 500 nm for n=1 and 580 nm for n=2. The absorbance differential peak at 580 nm of AKC-PAI film fit then with n=2 in good agreement with the XRD results. We have also measured the PL spectra of the AKC-PAI films. Above the main emission at 806 nm due to the 3D $Cs_{0.1}FA_{0.9}PbI_3$ phase of AKC, the spectrum of the treated sample presented an extra-emission at 570-580 nm (**Figure S11b,** Supporting Information) which agrees with the absorbance observation and confirms that the produced capping layer is mainly made of 2D $(PA)_2FAPb_2I_7$. Its formation can be described as follows: the surface 3D perovskite is partly dissolved by IPA and PAI reacts with the release compounds to form the 2D layer.[37] It is at the origin of recombination suppression at the PVK/HTL interface and then to the increased V_{oc} and *FF* parameters.

E. Effects of additives on the absorbance and photoluminescence of the $Cs_{0.1}FA_{0.9}PbI_3$ films.

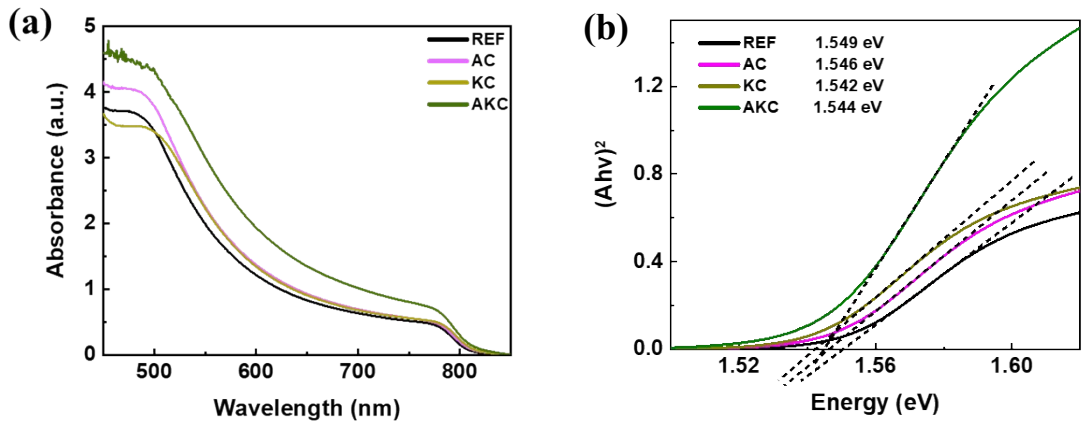

Figure S12. (a) Absorbance spectra of REF, AC, KC and AKC layers. (b) Tauc plot and bandgap determination.

Figure S16a compares the absorbance spectra of the optimized samples. Chloride additives are beneficial for the light absorption between 500 nm and 800 nm. The employment of each additive results in a stronger absorbance due to a better control of the film growth that produces covering and thicker layers. The best absorbance was obtained with the mixed additives. The absorption band-edge was analyzed by using Tauc plots in **Figure S16b** and the samples optical bandgap was determined. It was the same at about 1.54 eV whatever the precursor solution composition and no change was induced by K^+.

The recorded time-resolved photoluminescence curves (TRPL) of the samples are disclosed in **Figure 3m** and **3n**. At short times, the PL signal decreases more rapidly for the samples grown with single or mixed chloride additives. We have quantified the decay times by fitting the curves by a tri-exponential function and the fit results are reported in **Table S5**. The extracted emission short lifetime (τ_{fast}) was measured at about 3 ns for the REF sample and less than 1.9 ns for samples grown in the presence of one or two chloride additives. The three latter samples exhibited a similar behavior. It shows that, in the case of the REF sample, the electron injection is slower and more difficult.[37,44,46] The slow component, τ_{slow}, reported in **Table S5**, is assigned to recombinations occurring in the bulk perovskite.[44,47,48] It was measured at 168 ns for the reference and at 243 ns and 254 ns for the AC and KC films, respectively. It is conspicuous that both additives reduce the structural defects in the methylammonium-free perovskite. By mixing both AC and KC, we achieved a remarkable 551 ns value. It demonstrates that very high bulk perovskite quality was achieved then.

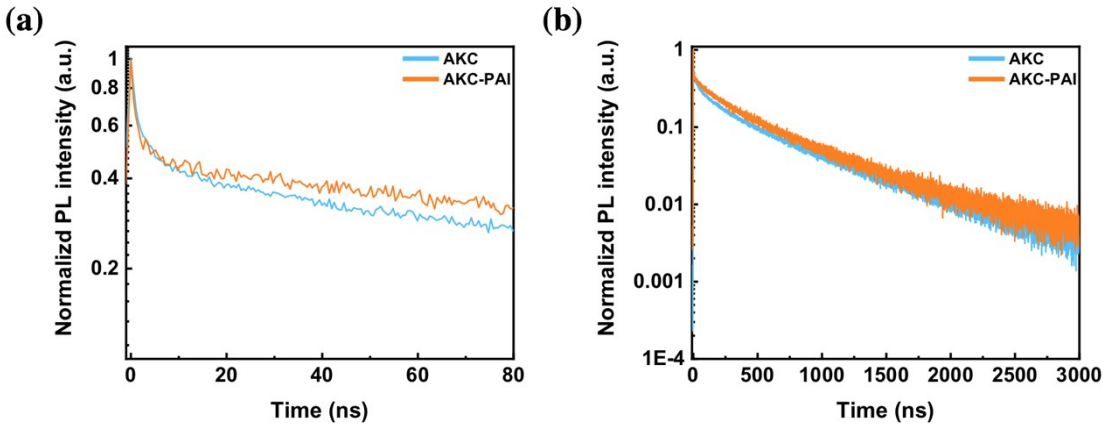

Figure S13. Effect of PAI post-treatment on the TRPL curves of PVK layers.

Table S5. Triple-exponential function fitting parameters of the TRPL decay curves measured at 472 nm on the series of optimized $Cs_{0.1}FA_{0.9}PbI_3$ films deposited on TiO_2.

Function : $y = A_1\exp(-x/\tau_1) + A_2\exp(-x/\tau_2) + A_3\exp(-x/\tau_3) + y_0$

Sample	y_0	A_1	τ_{fast} [ns]	RC_{fast}[a]	A_2	τ_{int} [ns]	RC_{int}[a]	A_3	τ_{slow} [ns]	RC_{slow}[a]
REF	7.8E-4	0.38	3.04	0.019	0.35	32.51	0.191	0.28	168	0.790
AC	1.59E-3	0.54	1.47	0.012	0.19	22.33	0.064	0.25	243.	0.923
KC	13.7E-4	0.49	1.58	0.009	0.16	36.21	0.066	0.32	254	0.925
AKC	29.1E-4	0.52	1.89	0.007	0.19	76.75	0.099	0.24	551	0.895
AKC-PAI	4.24E-3	0.51	1.21	0.004	0.17	110.15	0.108	0.27	570	0.888

[a] RC_{xx}: fast, intermediate and slow relative contributions.

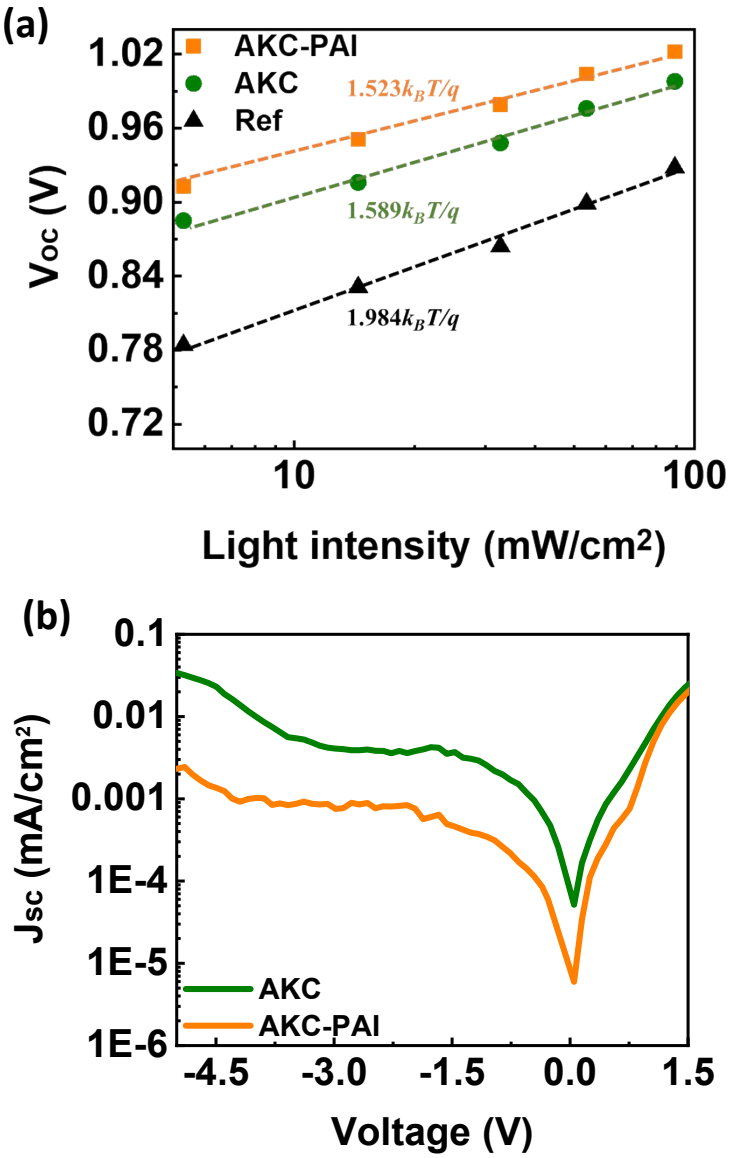

Figure S14. (a) V_{oc} versus light intensity (power density) curves of Ref cell (black dashed line), AKC cells without (green dashed line) and with (orange line) PAI post-treatment. (b) Dark current of AKC cell without (green trace) and with (orange trace) PAI treatment

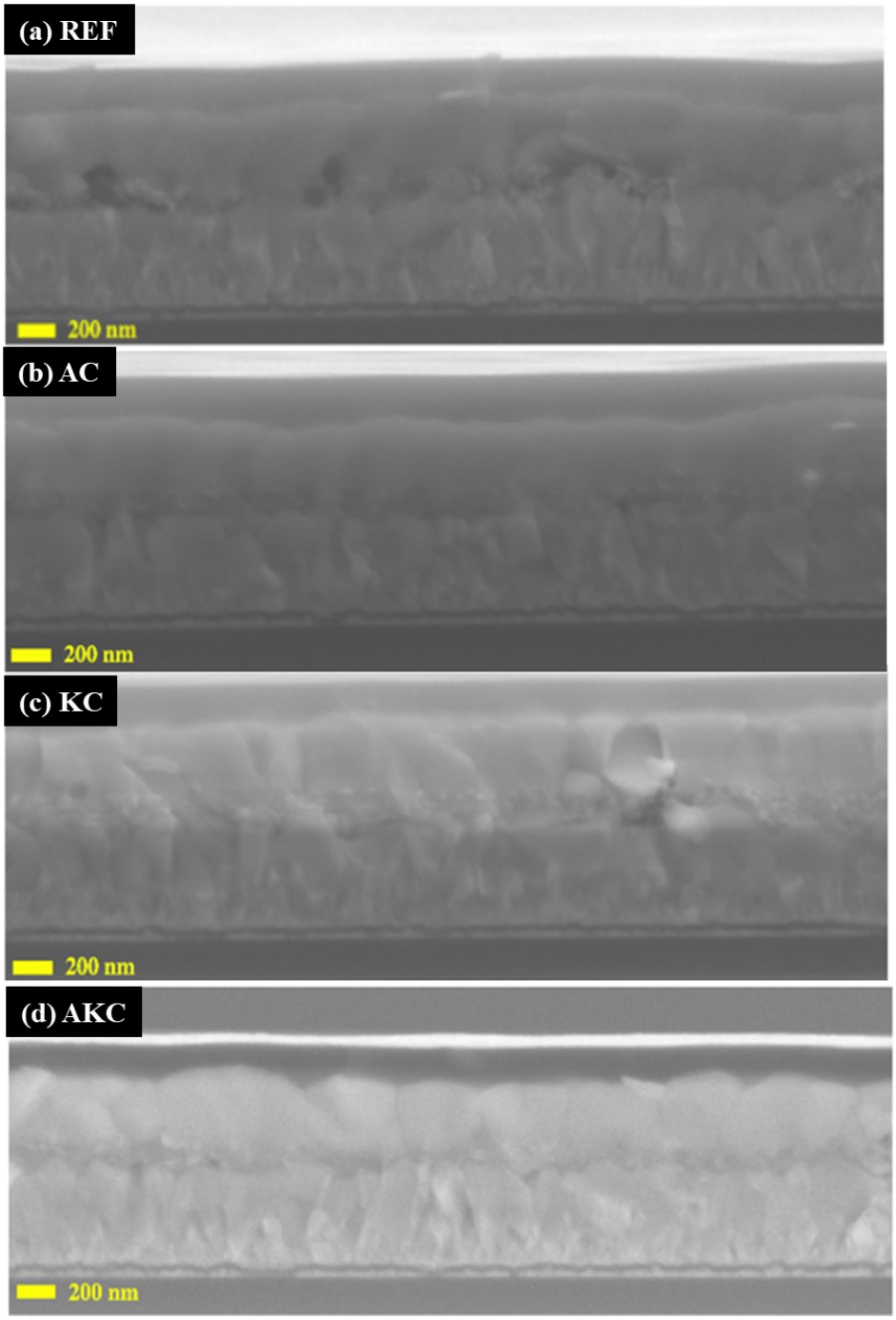

Figure S15. SEM cross sectional views of (a) REF, (b) AC, (c) KC and (c) KC/AC $Cs_{0.1}FA_{0.9}PbI_3$ layers deposited on glass/FTO/*c*-TiO2/*mp*-TiO_2 and topped with a spiroOMeTAD layer.

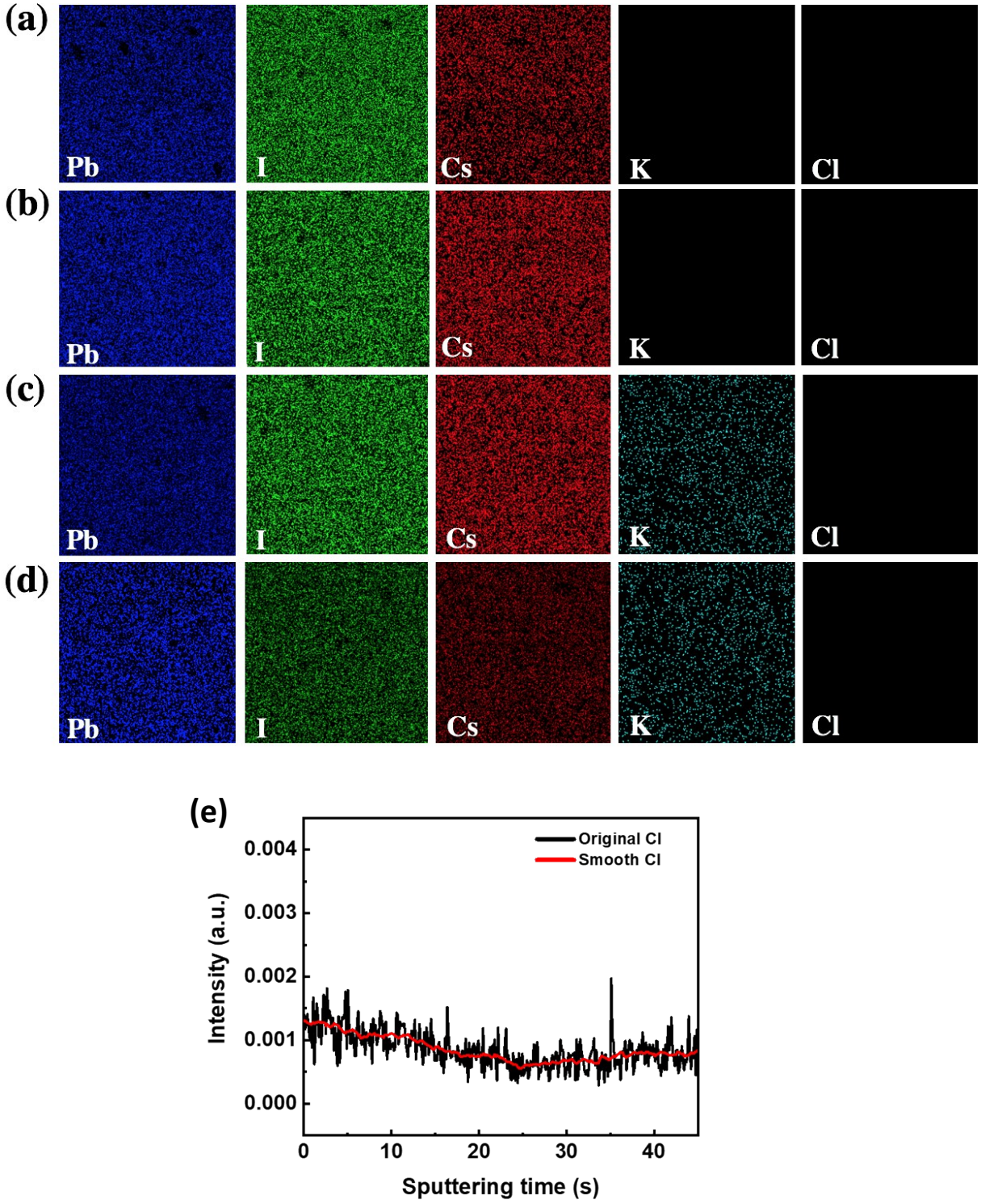

Figure S16. EDX elements mapping results of the perovskite layers. (a) w/o, (b) NH_4Cl, (c) KCl and (d) KCl/NH_4Cl. Size: 8 μm*8 μm. (e) GD-OES profile of Cl element in the KCl/NH_4Cl (AKC) PSC. The red trace is the smoothed curve.

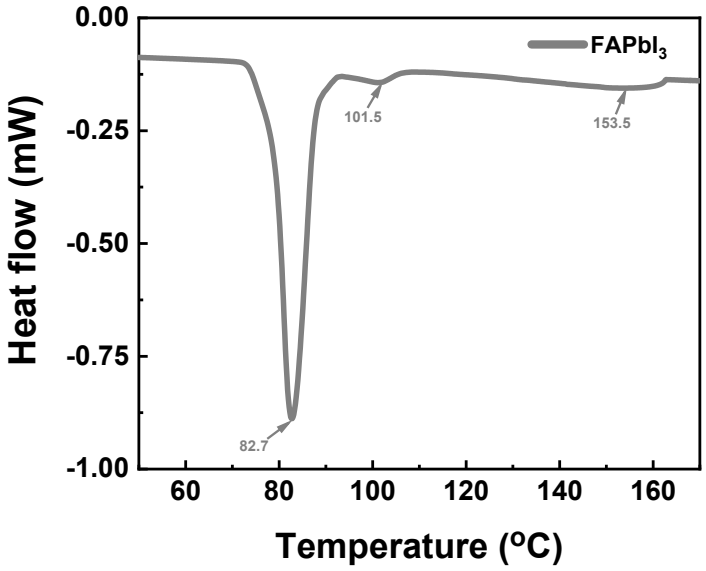

Figure S17. DSC curve of $FAPbI_3$ adduct.

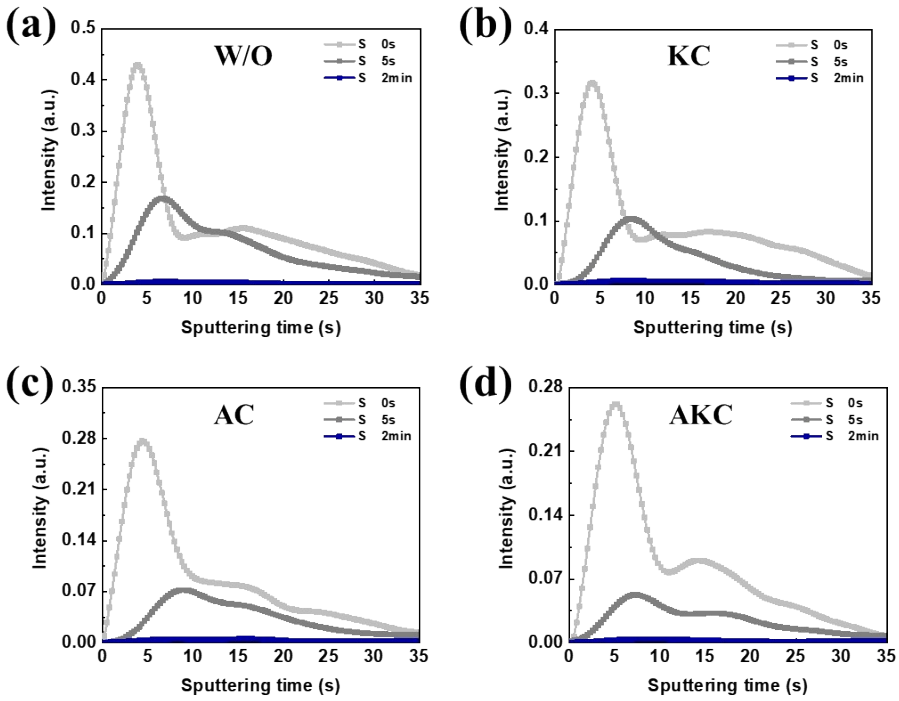

Figure S18. Effect of additives on the GD-OES S profile between 0 s and 2 min.

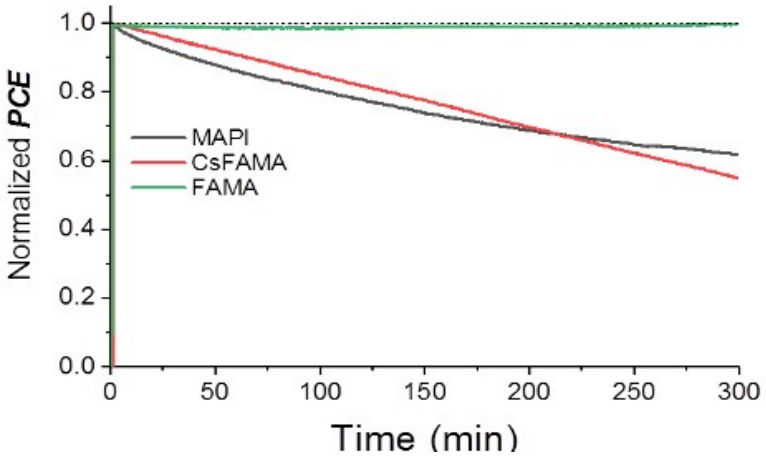

Figure S19 Tracking of $MAPbI_3$ (MAPI), $Cs_{0.08}FA_{0.80}MA_{0.12}Pb(I_{0.88}Br_{0.12})_3$, (CsFAMA) and $FA_{0.94}MA_{0.06}PbI_3$ (FAMA) solar cells normalized power outputs under continuous one sun AM1.5G illumination (unencapsulated devices 45% RH).

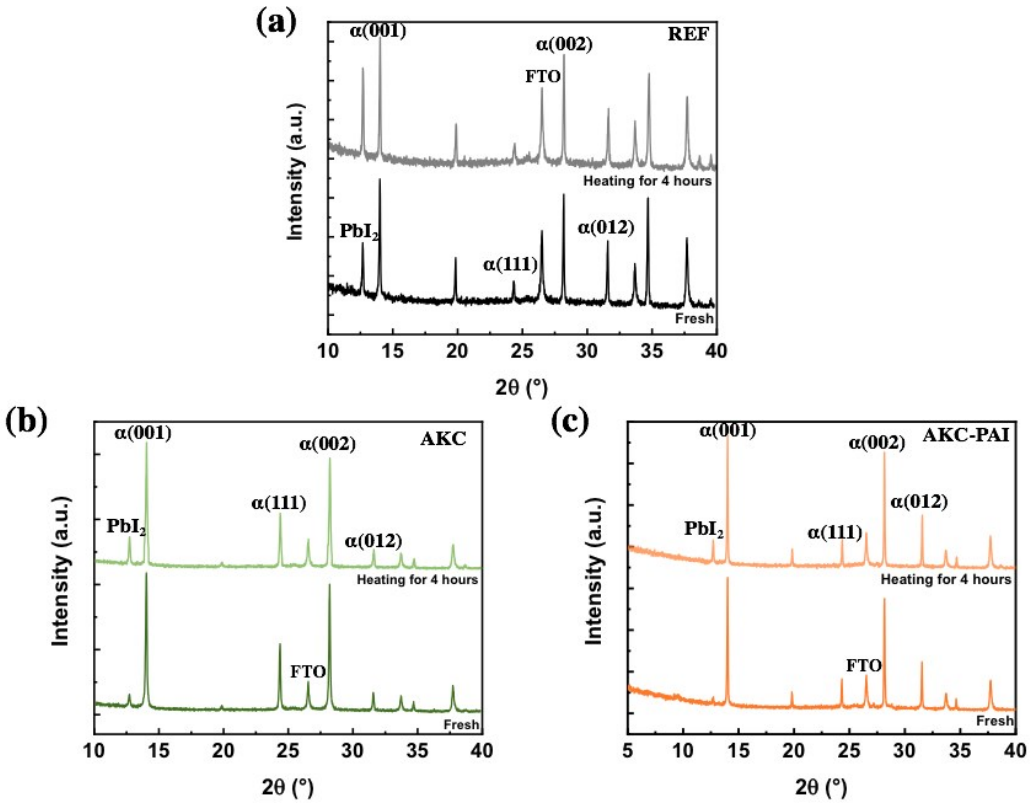

Figure S20. Effect of layer heating at 130°C for 4h on the XRD pattern of (a) REF, (b) AKC and (c) AKC-PAI layers.

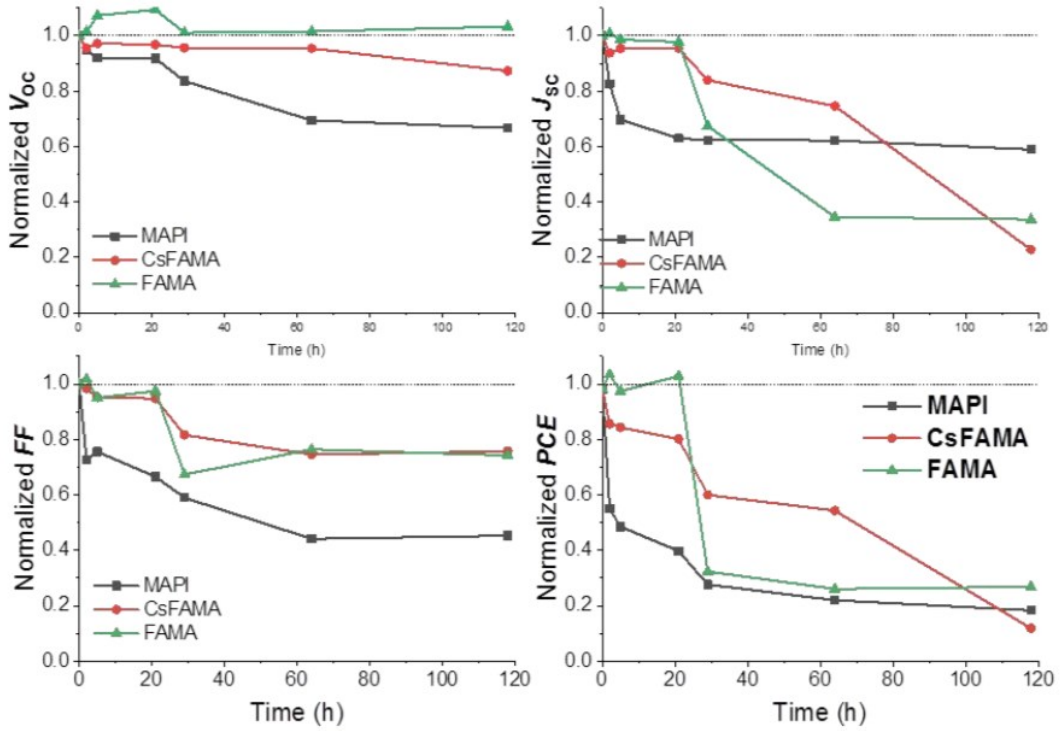

Figure S21. PCE and *J-V* curve parameters evolution of unencapsulated $MAPbI_3$ (MAPI), $Cs_{0.08}FA_{0.80}MA_{0.12}Pb(I_{0.88}Br_{0.12})_3$, (CsFAMA) and $FA_{0.94}MA_{0.06}PbI_3$ (FAMA) solar cells upon aging at 90 %RH.

F. Complementary Experimental

Preparation of the perovskite layers:

[$Cs_{0.1}FA_{0.9}PbI_3$] A perovskite precursor solution (PPS) with a 1.0M concentration was prepared by mixing 156 mg of Formamidinium iodide (FAI, greatcell), 461 mg of Lead iodide (PbI_2 , TCI) and 26 mg Cesium Iodide (CsI, TCI) in 900 µL DMF and 100 µL DMSO. The solutions were stirred for a minimum of 3-4h at 50 °C in a N_2 glovebox. 45 µL of this solution was placed on top of the substrates. A two-step spin-coating program was employed: first spinning at 1000 rpm for 10 s and then at 4000 rpm for 20 s. 100 µL of chlorobenzene was dripped 15~20 s after the starting of the spinning routine. The films were then annealed at 155 °C for 20 min. This film is noted REF.

[$Cs_{0.1}FA_{0.9}PbI_3$ with Ammonium Chloride] A PPS with a 1.0M concentration was prepared by mixing 156 mg of Formamidinium iodide (FAI, greatcell), 461 mg of Lead iodide (PbI_2 , TCI), 26 mg Cesium Iodide (CsI, TCI) and 5 mg, 10 mg, 15 mg, 20 mg and 25 mg (10 mol%, 20mol%, 30 mol%, 40 mol% and 50 mol%, respectively) of Ammonium Chloride (NH_4Cl, Alfa aesar) in 900 µL DMF and 100 µL DMSO. The films were spin-coated and annealed as before. These films and corresponding solar cells are noted AC-10, AC-20, AC-30, AC-40 and AC-50.

[$Cs_{0.1}FA_{0.9}PbI_3$ with Potassium Chloride] A PPS with a 1.0M concentration was prepared by mixing 156 mg of formamidinium iodide (FAI, greatcell), 461 mg of PbI_2 (TCI), 26 mg Cesium Iodide (CsI, TCI) and 3.7 mg, 6.7 mg, 9.7 mg (5 mol%, 9mol%, 13 mol%, respectively) of Potassium Chloride (KCl, Alfa aesar) in 900 µL DMF and 100 µL DMSO. The films were spin-coated and annealed as before. These films and corresponding solar cells are noted KC-5, KC-9 and KC-13.

[$Cs_{0.1}FA_{0.9}PbI_3$ with Potassium Chloride and Ammonium Chloride] A PPS solution with a 1.0M concentration was prepared by mixing 156 mg of Formamidinium iodide (FAI, greatcell), 461 mg of Lead iodide (PbI_2 , TCI), 26 mg Cesium Iodide (CsI, TCI), 10 mg and 15 mg (20 mol% and 30 mol%) of Ammonium Chloride (NH_4Cl, Alfa aesar) and 3.7 mg and 6.7 mg (5 mol% and 9 mol%) of Potassium Chloride (KCl, Alfa aesar) in 900 µL DMF and 100 µL DMSO. The films were spin-coated and annealed as before. These films and corresponding solar cells are noted KC-5/AC-20, KC-5/AC-30, KC-9/AC-20 and KC-9/AC-30.

[$(PA)_2PbI_4$] The PA-based 2D layer with n=1 was prepared by mixing 224 mg of Propylamine Hydroiodide (PAI, TCI) and 276 mg of Lead iodide (PbI_2, TCI) in 450 µL DMF and 50 µL DMSO to achieve a 1.2 M concentration precursor solution. The films were spin-coated and annealed as before. This film is noted $(PA)_2PbI_4$ (n=1).

[$(PA)_2FAPb_2I_7$] The PA-based 2D layer with n=2 was prepared by mixing 112 mg of Propylamine Hydroiodide (PAI, TCI), 52 mg of Formamidinium iodide (FAI, Greatcell) and 276 mg of Lead iodide (PbI_2 , TCI) in 450 µL DMF and 50 µL DMSO to achieve a 1.2 M concentration precursor solution. The films were spin-coated and annealed as before. This film is noted $(PA)_2FAPb_2I_7$ (n=2).

HTM layer and Gold Contact:

The hole transporting material (HTM) solution was prepared by dissolving 78 mg of Spiro-OMeTAD (Borun New Material Technology) in 1 mL of chlorobenzene. Then, 17.9 µL of bis(trifluoromethylsulfonyl)imide lithium salt solution (Li-TFSI) (Sigma Aldrich) solution (517 mg in 1 mL ACN), 30.4 µL of TBP (tert-butylpyridine) (Sigma Aldrich) and 14 µL of tris(2-1H-pyrazol-1-yl)-4-tert-butylpyridine)-cobalt(III) tris (bis(trifluoromethylsulfonyl)imide) (Dyesol, FK209) (376 mg in 1 mL acetonitrile) were added to this solution. 40 µL of the HTM solution was spin-coated at 4000 rpm for 30 s.[57] Finally, the device was completed by thermally evaporating a 70-80 nm thick gold back contact on the Spiro-OMeTAD layer.

***Synthesis of adduct powders*:**

First, 0.5 mL of precursor solutions were prepared by using the recipe mentioned above. Second, 10 mL of diethyl ether was added to precipitate the corresponding adduct. The precipitates were collected and dried in N_2 filled Glovebox overnight.